Title

Rates of β-amyloid deposition indicate widespread simultaneous accumulation throughout the brain

Authors

LaPoint, Molly R
Baker, Suzanne L
Landau, Susan M
et al.

Publication Date

2022-07-01

DOI

10.1016/j.neurobiolaging.2022.03.005

Peer reviewed

HHS Public Access

Author manuscript

Neurobiol Aging. Author manuscript; available in PMC 2023 July 01.

Published in final edited form as:

Neurobiol Aging. 2022 July ; 115: 1–11. doi:10.1016/j.neurobiolaging.2022.03.005.

Rates of β-amyloid deposition indicate widespread simultaneous accumulation throughout the brain

Molly R. LaPoint[a,*], **Suzanne L. Baker**[b], **Susan M. Landau**[a,b], **Theresa M. Harrison**[a], **William J. Jagust**[a,b]

[a]Helen Wills Neuroscience Institute, University of California Berkeley, Berkeley, CA 94720, USA

[b]Molecular Biophysics and Integrated Bioimaging, Lawrence Berkeley National Laboratory, CA 94720, USA

Abstract

Amyloid plaque aggregation is a pathologic hallmark of Alzheimer's disease (AD) that occurs early in the disease. However, little is known about its progression throughout the brain. Using Pittsburgh Compound B (PIB)-PET imaging, we investigated the progression of regional amyloid accumulation in cognitively normal older adults. We found that all examined regions reached their peak accumulation rates 24–28 years after an estimated initiation corresponding to the mean baseline PIB-PET signal in amyloid-negative older adults. We also investigated the effect of increased genetic risk conferred by the apolipoprotein-E ε4 allele on rates of amyloid accumulation, as well as the relationship between regional amyloid accumulation and regional tau pathology, another hallmark of AD, measured with Flortaucipir-PET. Carriers of the ε4 allele had faster amyloid accumulation in all brain regions. Furthermore, in all regions excluding the temporal lobe, faster amyloid accumulation was associated with greater tau burden. These results indicate that amyloid accumulates near-simultaneously throughout the brain and is associated with higher AD pathology, and that genetic risk of AD is associated with faster amyloid accumulation.

Keywords

Aging; Amyloid; Tau; APOE; Alzheimer's Disease; Longitudinal

1. Introduction

Amyloid-beta (Aβ) plaques are a hallmark of Alzheimer's disease and are also present in cognitively normal older adults. By their 70s, almost a third of older adults without cognitive impairment have extensive amyloid accumulation (Jack et al., 2008). Cognitively unimpaired individuals with abnormal levels of Aβ may have subtle brain and cognitive changes consistent with the presence of a "preclinical" phase of Alzheimer's disease (AD) (Sperling et al., 2011), and may be on an "Alzheimer's continuum" or have Alzheimer's disease based on biomarker categorization (Jack et al., 2018). Thus, identifying the earliest stages of Aβ accumulation may be key to detecting who is at the highest risk for developing

*Corresponding author at: Helen Wills Neuroscience Institute, University of California Berkeley, 132 Barker Hall MC#3190, Jagust Lab, Berkeley, CA 94720, USA, mlapoint17@berkeley.edu (M.R. LaPoint).

AD so that they can be followed closely, identified for clinical trials, and, if treatments become available, receive them in a timely manner.

Aβ can be measured in vivo using cerebrospinal fluid (CSF) and positron emission tomography (PET) with Aβ-sensitive radioligands. Often, studies assign participants to a "normal" or "abnormal" Aβ group based on cut points using CSF or a global PET measure which encompasses frontal, temporal, parietal, and cingulate cortices. This may be missing early stages of Aβ deposition when plaques may be present in only a subset of regions. Some studies have investigated the temporal progression of Aβ pathology, but the results have been inconsistent. Neuropathological studies typically show that association cortex deposition precedes medial temporal lobe (MTL), primary sensorimotor cortex, and subcortical areas (Braak and Braak, 1991; Thal et al., 2002), but the cortical regions shown to incur the earliest Aβ pathologic burden with neuroimaging vary in both cross-sectional (Cho et al., 2016; Grothe et al., 2017; Villeneuve et al., 2015; Yotter et al., 2013) and existing longitudinal studies (Guo et al., 2017; Jelistratova et al., 2020; Mattsson et al., 2019; Palmqvist et al., 2017).

The goal of this study was to use cross-sectional and longitudinal Aβ-PET data to examine the regional changes in amyloid deposition when individuals are still cognitively normal. First, we replicated a method used previously (Cho et al., 2016) to show regions where elevated amyloid was seen cross-sectionally. For these cross-sectional analyses, we predicted that frontal, parietal, and lateral temporal regions would show evidence of earlier Aβ accumulation than occipital, MTL, and sensorimotor regions. Identifying the earliest regions to display elevated Aβ might allow us to detect cognitively normal individuals who are at high risk for AD when measures of whole-brain Aβ burden are still below the threshold for positivity. This approach, combined with longitudinal measurements, could also reveal potential mechanisms underlying the spread of Aβ. For example, if amyloid deposits appear in 1 region years before depositing in functionally-connected regions, this may indicate spread occurs through functional networks. On the other hand, if Aβ appears in multiple regions at once, these regions may share certain tissue properties that affect their vulnerability to Aβ pathology (Whittington et al., 2018). After regional amyloid accumulation is staged, the relationship between regional amyloid accumulation and risk factors for AD and other pathologic markers of AD can be investigated.

One way to study longitudinal amyloid change is to examine the relationship between baseline Aβ burden and rate of change in Aβ burden, which is a quadratic function when measured globally (Blautzik et al., 2017; Jack et al., 2013; Jagust and Landau, 2021; Villemagne et al., 2013). Using the quadratic equation representing this association, we can calculate a sigmoidal relationship between Aβ accumulation and time. The present study used this approach to investigate associations between regional slope and baseline global PET values to find the time course over which different regions reach their peak accumulation rates. The results from these longitudinal analyses were compared to a previous cross-sectional staging method (Cho et al., 2016). In addition, 2 previous studies have created a sigmoidal relationship between regional amyloid accumulation and time, one with modeled cross-sectional data (Whittington et al., 2018) and one with longitudinal data (Insel et al., 2020) and both show results that appear to be inconsistent with long-term

spread of Aβ from one region to another. We, however, predicted that frontal, parietal, and lateral temporal regions would reach their peak accumulation rate before occipital and MTL regions, but that most association cortex regions would show similar timing in Aβ accumulation.

In the process of examining rates of regional Aβ accumulation, we also investigated the most important genetic factor involved in late onset AD, the Apolipoprotein E (*APOE*) genotype. Individuals with the ε4 allele are more likely to develop sporadic AD. In cognitively normal cohorts, ε4 carriers have been shown to have higher levels of Aβ pathology than noncarriers (Fouquet et al., 2014; Resnick et al., 2015). However, studies of longitudinal Aβ accumulation rates in ε4 carriers and noncarriers are inconsistent, with some finding no significant difference in accumulation rates and others showing higher accumulation rates in ε4 carriers than noncarriers. (Burnham et al., 2020; Lim and Mormino, 2017; Mishra et al., 2018; Resnick et al., 2015). It is unclear if ε4 carriers simply develop Aβ earlier than noncarriers, but accumulate at the same rate, or if accumulation rate itself is faster in carriers versus noncarriers. Here we investigate the relationship between regional accumulation rates of Aβ in ε4 carriers and noncarriers, controlling for baseline levels of pathology in each region. We predicted that ε4 carriers would have faster accumulation rates in regions found to accumulate Aβ earlier (frontal, parietal, and lateral temporal regions) versus ε4 noncarriers.

Finally, we were interested in the association of Aβ accumulation with another pathologic hallmark of AD, tau pathology. In contrast with Aβ, tau pathology accumulates following a stereotyped pattern beginning in the MTL (where high tau is common in older age), progressing to the surrounding inferolateral temporal lobes, and then spreading throughout the remaining cortex (Schöll et al., 2016; Vogel et al., 2020). Tau and Aβ burden are positively correlated in animal (He et al., 2018) and human studies (Lockhart et al., 2017; Vemuri et al., 2017) and individuals who have high levels of both are more likely to develop dementia (Pascoal et al., 2017).

The mechanisms by which high levels of tau and Aβ interact to create or contribute to cognitive decline are still unclear, especially since the regions susceptible to early tau, and Aβ deposition do not overlap. While relationships between cross-sectional PET measures of Aβ and tau have been explored (Lockhart et al., 2017), there are no data examining how the regional rates of Aβ deposition may lead to regional tau deposition. Thus, we sought to investigate the relationship between Aβ accumulation rates and cross-sectional tau-PET proximate to the final Aβ measurement, within, and between regions. By creating a map of early Aβ-depositing regions, we were able to investigate the relationships between regional accumulation rates and increased tau, both local, and distant. We predicted that MTL tau would be associated with rates of Aβ accumulation in all regions, but that tau pathology outside the MTL would only be associated with accumulation in early Aβ regions.

Therefore, our study seeks to increase understanding of how the time course of Aβ accumulation varies by region, whether these accumulation rates differ in those with genetic risk for sporadic AD, and how accumulation rates in regions with different time courses associate with tau pathology in AD.

2. Materials and methods

2.1. Participants

We recruited 195 participants from the Berkeley Aging Cohort Study (Mormino et al., 2009). All participants were cognitively normal, over 60 years of age, and had at least 1 [^{11}C] Pittsburgh compound B (PIB) Positron emission tomography (PET) scan for measurement of Aβ. A subset of 106 participants had more than 1 PIB-PET scan and were used for longitudinal analyses. Eighty-eight of these 106 participants had at least 1 [^{18}F] Flortaucipir (FTP) PET scan to measure tau pathology proximal to their final PIB-PET scan. All but 10 participants had FTP and PIB-PET scans on the same day and the median date difference was 0 days. Across all scans, the median difference between the PIB-PET and MRI scan was 8 days. Participant characteristics can be found in Table 1. Amyloid positive individuals were selectively recruited for longitudinal studies, producing an uncharacteristically high rate of amyloid positivity.

2.2. Image acquisition

[^{11}C] PIB was synthesized at Lawrence Berkeley National Lab (LBNL) Biomedical Isotope Facility as previously described (Mathis et al., 2003). PIB-PET imaging was carried out on 1 of 2 scanners, the ECAT EXACT HR or the BIOGRAPH PET/CT Truepoint 6. Previous studies have shown that there is no significant difference in distribution volume ratios (DVRs) between the 2 scanners (Elman et al., 2014).

Details of PIB-PET scan acquisition have been previously outlined (Lockhart et al., 2017). Subjects received an intravenous injection of PIB (~15 mCi), at the beginning of 90 minutes of dynamic acquisition frames. The data were binned into 35 frames (4 × 15 seconds, 8 × 30 seconds, 9 × 60 seconds, 2 × 180 seconds, 10 × 300 seconds, and 2 × 600 seconds). A transmission or CT scan was acquired immediately before the emission scan for attenuation correction.

[^{18}F]FTP-PET was synthesized at LBNL based on a protocol provided by Avid Radiopharmaceuticals as previously described (Schöll et al., 2016). FTP scans were done on the BIOGRAPH scanner. Data acquired from 80 to 100 minutes post-injection were binned into 4 × 5-minute frames during reconstruction and used in subsequent analyses.

All PET images were reconstructed using an ordered subset expectation maximization algorithm with weighted attenuation, scatter correction, and smoothed with a 4mm Gaussian kernel. Participants also underwent MRI on a 1.5 Tesla Siemens Magnetom Avanto MRI scanner at LBNL. A FreeSurfer (FS; http://surfer.nmr.mgh.harvard.edu/) version 5.3 segmentation of a T1-weighted magnetization prepared rapid gradient echo (MPRAGE) scan (TR/TE = 2110/3.58 ms, FA = 15°, 1 × 1 × 1 mm resolution) was to used parcellate PET scans into regions of interest (ROIs) for analysis of PET images.

2.3. Image processing

2.3.1. PIB-PET—PIB-PET data were realigned, resliced, and coregistered to correspond to their closest structural scan from the 1.5 T MRI. There was a median of 7 days between

the scans (range 0–767 days). Logan graphical analysis was used to calculate the DVR values as the slope of frames 35–90 minutes post-injection with a cerebellar reference region (Logan et al., 1996; Price et al., 2005). The structural MRI corresponding to each PET scan was processed with FS to derive ROIs in native space for each subject using the Desikan-Killiany atlas. The PET image was coregistered to the MRI, allowing us to calculate mean regional DVR values for each FS ROI. The global cortical PIB measure was calculated in native space for each participant (Mormino et al., 2011). In addition, the following FS regions were averaged to form larger composite cortical regions: lateral parietal (superior parietal, supramarginal, inferior parietal), medial parietal (precuneus, isthmus cingulate, posterior cingulate, paracentral), lateral frontal (rostral middle frontal, caudal middle frontal, pars orbitalis, pars triangularis, pars opercularis), medial frontal (superior frontal, caudal anterior cingulate, rostral anterior cingulate), orbitofrontal (OFC; frontal pole, medial and lateral orbitofrontal) sensorimotor (precentral and postcentral), inferior lateral temporal (fusiform, inferior and middle temporal), superior lateral temporal (superior temporal, transverse temporal, banks of the superior temporal sulcus), insula (insula), MTL (entorhinal and parahippocampal) and occipital (lateral occipital, lingual, cuneus, pericalcarine).

2.3.2. FTP-PET—FTP Standardized Uptake Value Ratio (SUVR) images were generated based on mean tracer uptake 80–100 minutes post-injection using an inferior cerebellar gray matter reference region (Baker et al., 2017a). Like the PIB-PET data, the images were coregistered, and resliced to each subject's 1.5 Tesla MR scan closest to the FTP scan. The scans occurred, on average, 30 days apart. SUVR images were partial volume corrected using the Geometric Transfer Matrix approach on FreeSurfer-derived values (Baker et al., 2017b; Rousset et al., 1998). The same composite ROIs were calculated for FTP as for PIB.

2.4. Statistical analysis

Statistical Analyses were conducted using MATLAB version 9.4 (R2018a; MathWorks, Inc, Natick, Massachusetts) and R version 3.4 (https://www.R-project.org/), including the packages *nlme* for analyses and *ggplot2* and *ggseg3d* for data visualization.

2.4.1. Cross-sectional PIB staging analyses—We used cross-sectional data to infer a pattern of temporal progression of Aβ deposition, similar to methods used by others in staging Aβ pathology (Cho et al., 2016) in order to determine the ordering of positivity between regions, and to allow for comparison with the longitudinal methods. Mean and standard deviation values for each region were calculated in the subset of participants below the cutoff for PIB positivity (N = 122; DVR <1.065; Villeneuve et al., 2015). These values were used to Z-score each region's data for the entire sample. For each region, the number of participants with a Z-score >2.5 was counted, and regions were ranked from those with the highest proportion of individuals with Z-scores >2.5 to those with the lowest. Ties were broken by calculating the mean value of the Z-scores, with higher Z-score means leading to a higher ranking.

2.4.2. Longitudinal PIB staging analyses—A linear function of DVR versus time was used to characterize the annual rate of change for subsequent analyses that minimized

distance from the regression line (Leal et al., 2018). Next, linear and quadratic models were fit in R using annual accumulation rate for each region (along with global PIB slope) and baseline global PIB values. In the linear model (slope ~ BL global PIB), regional slope was the dependent variable, and global PIB was the independent variable. The quadratic model included the same parameters, but also included a baseline global PIB squared term (slope ~ BL global PIB + BL global PIB$^{2)}$. For regions where both baseline global PIB terms were significantly associated with slope, Aikake Information Criterion (AIC), and residual sum of squares were used to compare the fit.

For regions where the quadratic model was a better fit, the maximum of the quadratic equation (created using the estimates from the model) could be found algebraically: for the function $f(x) = ax^2 + bx + c$, the maximum point is $(-b/(2a), f(-b/(2a))$. The x coordinate represents the global PIB DVR at which this region's PIB accumulation rate is fastest. Because all equations used baseline global PIB DVR as the independent variable, the global DVRs at which each region reaches its peak accumulation can be directly compared.

We next calculated the annual change in global DVR starting from the mean baseline global PIB DVR for PIB negative participants (DVR = 1.02). Annual change was calculated using the quadratic function through a time course of 50 years (Jagust and Landau, 2021). We also converted DVR values to Centiloids (CLs), a standardized scale allowing for comparison of results using different Aβ-PET radiotracers (Klunk et al., 2015). This approach enabled us to determine when accumulation in a region starts to decelerate.

2.4.3. PIB-APOE associations—Participants were categorized as carriers or noncarriers of the APOE ε4 allele. Because noncarrier longitudinal accumulation data did not fit quadratic models, linear mixed effects models (LME models) carried out using the R package *nlme* were used for these analyses to compare the linear trajectories of the carriers and noncarriers. In these models, PIB-PET was the dependent variable, with fixed effects APOE status, age, and sex, all interacting with time. The random effects were (1+time|subject) which modeled a subject-specific intercept and allowed the results to vary by subject over time.

2.4.4. Amyloid-tau associations—Relationships between PIB-PET accumulation rates and FTP-PET within and across ROIs were examined using LMEMs. In these models FTP-PET was the dependent variable, with fixed effects PIB-PET, age, and sex as well as their interactions with time. The random effects were (1+time|subject). Local and distant analyses were run for all regions, as well as analyses examining the association between global PIB accumulation rate, and regional tau. All statistics are reported at a liberal threshold of $p < 0.05$, uncorrected.

3. Results

3.1. Cross-sectional results

The results of the cross-sectional analysis can be found in Table 2. There were small differences in the proportions of participants with abnormal values in frontal and parietal

cortex. Regions with the lowest proportion of abnormal subjects were sensorimotor, MTL, and occipital.

Fig. 1 shows these results graphically for each participant. Global PIB-PET captured the greatest number of people with elevated Aβ pathology. Furthermore, most participants were either above the cut points in all or nearly all regions or were not above the cut point in any region. Taken together with the finding that global PIB had the most participants above a Z-score of 2.5, this indicates that although some individuals show regionally specific PIB-PET signal, levels of PIB do not considerably differ by region.

3.2. Longitudinal results

Quadratic Model Fit—Quadratic models better fit the data in 8 of 11 regions and global PIB. The global PIB value at which each region reaches its fastest rate of accumulation, as well as the average rate of accumulation for each region, can be seen in Table 3. Neither the fastest accumulating (OFC; 0.014 DVR/year) or the slowest accumulating (MTL; 0.003 DVR/year) fit a quadratic. The first region to reach its peak accumulation rate was lateral parietal. Insula was the final one, with a difference in DVR of 0.13, CL value of 17, and an estimated time difference of 2–4 years. The quadratic fits for a subset of regions are plotted in Fig. 2.

3.2.1. Regional PIB time course—

Given a starting point of the mean global PIB value for PIB negative participants (DVR = 1.02; CL = 4), it would require 8–9 years to reach the threshold for PIB positivity (DVR = 1.065; CL = 10). The time course of global PIB accumulation can be seen in Fig. 3, with the points at which select regions reach their peaks superimposed on the global PIB graph.

3.3. PIB-APOE relationships

In all models, APOE status was significantly associated with PIB-PET, both in its own term, and interacting with time. Visualization showed that ε4 carriers had higher PIB-PET at baseline, and it increased at a slightly faster rate. Results of these models are listed in Table 4 and a subset of associations between ε4 carrier status and regional slope are shown in Fig. 4.

3.4. Tau-amyloid relationships

Relationships between longitudinal PIB accumulation and FTP looked similar, regardless of the PIB region in LMEs (Fig. 5). Local relationships were only seen between PIB accumulation rates and FTP in the lateral parietal (t [157] = 2.28, $p = 0.024$), superior lateral temporal (t [157] = 2.19, $p = 0.029$) and occipital regions (t [157] = 2.70, $p = 0.0078$). For most PIB regions, accumulation rate was most strongly associated with temporal FTP, especially lateral temporal regions, and lateral parietal FTP. PIB accumulation rates measured globally, and in medial parietal and OFC, were most strongly associated with FTP in temporoparietal brain regions, and also were associated with a wider distribution of FTP. Notably, these PIB regions, along with global PIB, were the 4 PIB measures with the highest percent involvement of PIB in cross-sectional methods, and among the fastest accumulation rates.

Furthermore, PIB accumulation in the medial, and inferior lateral temporal lobe was not associated with FTP in any region. Both regions had lower percent involvement of PIB in cross-sectional methods; inferior lateral temporal was one of the last regions to reach its peak accumulation rate in the quadratic analyses.

4. Discussion

In this study, we investigated global rates of regional Aβ accumulation, and examined whether dynamics of Aβ accumulation in different brain regions differed from one another. This focus on both global and regional rates of Aβ accumulation allowed us to determine another measure of regional vulnerability to Aβ and permitted us to see how regional rates of Aβ accumulation related to APOE genotype and tau deposition. As anticipated, cross-sectional results showed that global PIB-PET signal captured the most individuals with elevated Aβ. Those with high levels of PIB-PET in one region were likely to have high PIB-PET in most regions, but small differences between regions indicated that high levels of Aβ were most common in frontal and parietal regions, and least common in temporal cortex (particularly the MTL), the occipital lobe, and sensorimotor cortex. In longitudinal analyses, all investigated regions reach their peak accumulation rate within a span of 4 years (24–28 years after accumulation began), indicating that spread from one region to another is unlikely, although, as discussed below, this inference is subject to some limitations. Compared to noncarriers, APOE ε4 carriers had higher baseline Aβ, and faster accumulation in all regions even after controlling for regional baseline Aβ. Lastly, faster Aβ accumulation was associated with elevated tau in temporal and parietal regions. These relationships were stronger and more widespread in the brain regions that deposited Aβ more rapidly, and no relationships were seen between Aβ accumulation in MTL or inferior lateral temporal regions and tau pathology in any region. Together, these results further our understanding of the regional dynamics of Aβ accumulation in unimpaired older adults and show how the rate of accumulation relates to genetics and tau pathology.

4.1. Regional amyloid deposition

In the present study, there were regions that were more likely to harbor amyloid deposition than others, but most regions seemed to accumulate amyloid at a similar rate. Cross-sectionally, frontal and parietal regions were more likely to harbor elevated Aβ, and MTL sensorimotor, and occipital regions were less likely. Elevated Aβ in one region, however, was typically indicative of elevated Aβ throughout much of the cortex. These results are consistent with autopsy studies, in which frontal, parietal, and lateral temporal regions consistently show Aβ plaques before MTL and primary sensorimotor cortex (Braak and Braak, 1991; Thal et al., 2002). Cross-sectional Aβ-PET data show that deposition of Aβ in the sensorimotor cortex, occipital lobe, and medial temporal regions is less at early stages of AD (Cho et al., 2016; Grothe et al., 2017; Yotter et al., 2013). Our findings using the methods from Cho et al. (2016) largely replicate their results and add to a body of literature showing elevated Aβ in neocortical association areas with fewer individuals harboring high Aβ in MTL, sensorimotor, and occipital regions.

Cross-sectional results, however, do not address whether brain regions accumulate Aβ at different rates. In our longitudinal analyses, we found that all regions reached their peak accumulation rates 24–28 years after accumulation begins. A benefit of the present study is that, since accumulation in all regions was fitted to a quadratic with baseline global Aβ, we could directly compare the timing of accumulation. We found that, although some regions might accumulate Aβ slightly earlier or more quickly, the temporal differences between regional rates of Aβ accumulation are small. Many studies of regional Aβ have created staging schema using various methods. Some studies use cutoffs to identify regions that are elevated more often. One such study identified basal portions of the temporal lobe, the anterior cingulate, and parietal operculum as the earliest regions of deposition, with large portions of the frontal, parietal, and temporal lobes following in the second stage (Grothe et al., 2018). Although this staging method was created with cross-sectional data, it has been verified longitudinally (Jelistratova et al., 2020; Teipel et al., 2020). Others identify participants as Aβ accumulators or non-accumulators with the help of CSF measurements of Aβ, and compare where Aβ is highest, or where it is increasing fastest in accumulators versus non-accumulators. In these studies, earliest-stage Aβ appeared in the medial parietal lobe, medial frontal, and orbitofrontal cortex, with one additionally identifying lateral temporal regions (Mattsson et al., 2019; Palmqvist et al., 2017). Studies have also investigated either regions where participants have a high Aβ burden compared to their global Aβ value, or simply regions where either baseline Aβ burden is highest or where Aβ burden is increasing the fastest. Highest baseline values and fastest rates of change are often seen in the precuneus, anterior and posterior cingulate, and lateral frontal regions (Guo et al., 2018, 2017; Insel et al., 2020). What is typically consistent, however, is that medial temporal, occipital, and sensorimotor regions are among the final regions to become involved (Grothe et al., 2017; Guo et al., 2018, 2017; Mattsson et al., 2019; Palmqvist et al., 2017). Previous studies have often used clinically diverse cohorts including cognitively impaired participants. The wide array of regions that may define early stages of Aβ deposition may be due to demographic differences and/or PET radiotracer properties magnifying small differences in different cohorts.

This study is largely consistent with previous studies modeling the time course of Aβ over a sigmoidal trajectory. Important time points found in this paper and 3 others can be found in Table 5. Besides the present study, all other papers included cognitively impaired patients in their analyses (Jack et al., 2013; Jagust and Landau, 2021; Villemagne et al., 2013), and Villemagne et al. used mean PIB rather than baseline PIB. Despite these differences, the temporal patterns are surprisingly similar. From a starting point of the mean Aβ burden of CNs, in the present study it would take 28–29 years to reach a typical Aβ burden for AD patients (equivalent to a CL value of 100), versus 28 years in ADNI (Jagust and Landau, 2021) and 31 years in AIBL (Villemagne et al., 2013). The time course in AIBL is very similar to the present study, with only the time to the Aβ positivity threshold more than approximately 2 years longer (12 years vs. 8–9 years). In ADNI the starting point for the sigmoid is the same as the present study (4 CL) and the overall time course is very similar, but the amount of time it takes to reach the peak accumulation rate from the Aβ positivity threshold is much shorter (3 years vs. 17–18 years) and the time to reach an average AD patient value from that peak is much longer (18 years vs. 3–4 years). This may be due

to the high number of cognitively impaired participants in the ADNI study (>60%) along with the requirement that only controls with positive amyloid-PET slopes were included. Data from the Mayo Clinic Study of Aging (MCSA) are somewhat difficult to compare because the starting SUVR for inclusion was higher. Perhaps for this reason, timing from a positive scan (an SUVR of 1.5) to a value typical of an AD patient required only about 14 years. Across all studies the most variable period of accumulation seems to be from the Aβ positivity threshold to the peak, which included values of 3, 6.6, and 18 years. Differences may be related in part to Aβ tracer used, or methodological differences in PET processing (such as the chosen reference region). This is a dynamic phase of Aβ accumulation and the inverted-U relationship is variable across studies, and any time course is relative to a study-defined starting point, so differences likely also reflect cohort composition.

Two papers have modeled sigmoidal trajectories for regional Aβ (Insel et al., 2020; Whittington et al., 2018). As in this report, which modeled trajectories of regional accumulation relative to global Aβ so regional time courses can be compared on the same time scale, these results found limited differences in accumulation between regions. Insel and colleagues modeled accumulation of Aβ in different brain regions as a function of estimated disease time, and found that some regions, such as the precuneus and posterior cingulate, begin with high uptake and continue to increase in Aβ-PET uptake over time; other regions (lateral OFC, isthmus cingulate, inferior parietal) start high but increase more slowly; in this report, all regions appear to reach their inflection point around the same time. This is similar to the findings of an earlier paper modeling accumulation with cross-sectional data, which concluded that amyloid accumulation begins simultaneously throughout the brain and that all regions reach their peak accumulation rates around the same time, with differences in the rate of accumulation based on carrying capacity (Whittington et al., 2018). This may help explain the somewhat surprising finding that sensorimotor cortex was one of the regions to reach its peak accumulation rate earlier despite relatively low levels of Aβ. This contrast between rapid accumulation rates and low values of Aβ may reflect 2 distinct processes, such that vulnerability may reflect either the rate of accumulation or the resulting amount of pathology.

The overall similarities of our results with these previous studies, despite using only cognitively normal older adults, is notable. The time course appears to be elongated in the present study, which is not surprising given the entirely cognitively normal sample. The trajectory may be longer than in a sample of individuals who either have probable AD dementia or are likely to develop it (those with MCI, cognitive deficits, high Aβ, accelerating Aβ accumulation, etc.). However, it is useful to investigate the time course of Aβ in a cognitively normal sample as well. Many of these individuals are amyloid positive and so are considered to be on the Alzheimer's continuum; while we did not dichotomize tau outcomes, some would also be classified as having biomarker evidence of Alzheimer's disease according to the current research framework (Jack et al., 2018). Understanding the earliest stages of Aβ, before cognitive impairment, may be crucial to early treatment of the disease, and this time course would be harder to parse if patients were included in the model.

Overall, these results indicate that significant inter-region spread of Aβ, through functional connections or otherwise, is not likely, given the short time differences between each

region's peak accumulation rate. This seems especially unlikely when taking into account the variability in early-stage regions seen *post mortem* (Braak and Braak, 1991; Thal et al., 2002) and PET studies of regional Aβ (Guo et al., 2018; Mattsson et al., 2019; Sakr et al., 2019). This is also consistent with the frequent finding that in large samples, Aβ positive and Aβ negative participants dominate, with few intermediate individuals, consistent with widespread and rapid increases in Aβ in vulnerable individuals and regions. This stands in contrast with tau pathology, which is mainly restricted to MTL regions in older adults without cognitive impairments, seeming to spread to nearby temporal lobe locations and functionally-connected regions in the presence of higher Aβ over longer time periods and through documented networks of connectivity (Adams et al., 2019; Franzmeier et al., 2020; Schöll et al., 2016; Vogel et al., 2020). However, we recognize that our models depend on Aβ that can be visualized with PET. It is possible that soluble forms of Aβ, or even fibrillar forms at very low and undetectable levels, may spread through connectivity many years before signal can be detected with a PET scan. Furthermore, it is possible that network-based spread could happen extremely quickly.

It seems most likely that regions which accumulate Aβ earlier share factors that make them vulnerable to aggregated Aβ peptide accumulation. They may, for example, have similar properties. In a study of regional gene expression, higher expression of the Aβ precursor protein (APP) gene, and reduced expression of genes involved in protein synthesis and mitochondrial respiration are associated with higher levels of Aβ-PET (Grothe et al., 2018). Patterns of regional metabolism are also implicated based on data showing that amyloid accumulating regions are involved in aerobic glycolysis (Vlassenko et al., 2010) and that they have lifelong elevated levels of glucose metabolism (Oh et al., 2016). These genetic and metabolic factors are likely to drive shared vulnerability resulting in Aβ aggregation appearing almost simultaneously in susceptible regions.

4.2. APOE E4-regional Aβ accumulation relationships

In this study, we also found that carriers of the APOE ε4 allele had faster accumulation of Aβ than noncarriers in all brain regions, adjusting for the difference in baseline Aβ. Our results are consistent with studies that report faster rates of accumulation in carriers (Burnham et al., 2020; Lim and Mormino, 2017; Mishra et al., 2018), although there are discrepancies (Lopresti et al., 2020; Resnick et al., 2015) Burnham et al (2020). and Lim and Mormino (2017) both noted effects of APOE ε4 genotype early in the stage of Aβ deposition, prior to reaching an amyloid positivity threshold. Thus, it is possible that the ε4 allele shifts the onset of Aβ deposition by subtly increasing rates prior to reaching an amyloid positive stage.

4.3. Regional amyloid-tau relationships

Longitudinal associations between Aβ accumulation and tau mirrored the relationships found in our previous report with cross-sectional data (Lockhart et al., 2017) and were also similar to the pattern of elevated tau seen in studies investigating longitudinal global Aβ and tau (Tosun et al., 2017). Faster PIB accumulation in most regions was associated with cross-sectional FTP-PET in a relatively limited group of brain regions, with strongest relationships seen between PIB in multiple regions and FTP in the temporal lobe, where pathologic

tau is known to accumulate early in AD (Braak and Braak, 1991; Johnson et al., 2016; Schöll et al., 2016). Nevertheless, there were some regional associations between rates of Aβ accumulation and tau deposition, with no association between Aβ accumulation in inferior lateral and media = l temporal lobes and tau pathology, and stronger associations between Aβ accumulation in faster accumulating regions (OFC and medial parietal cortex) and tau pathology. The fact that regional Aβ accumulation was associated with a similar pattern of tau—especially temporal tau—is consistent with interpretations of prior cross-sectional data indicating that tau and Aβ pathology start in different regions, and that the location of Aβ accumulation bears non-specific relationship to the location of tau pathology both within and outside the temporal lobe. The similar findings for both cross-sectional and longitudinal Aβ accumulation raise crucial unanswered questions about how the widespread pattern of Aβ accumulation drives a relatively more focal deposition of tau pathology.

4.4. Limitations

There are some limitations to the present study. The sample size is relatively small, compared to some studies. About half of the participants have only 2 PIB-PET time points, whereas it is optimal for longitudinal analyses to have 3 or more time points. In addition, all participants in the cohort are cognitively unimpaired. This is partially a strength and is helpful for characterizing early pathologic changes and as previously mentioned, verifying that Aβ accumulation in CN older adults follows a quadratic shape. However, it has drawbacks, such as limiting the number of high-Aβ ε4 noncarriers. Our ability to extrapolate to the full spectrum across the natural history of AD is thus limited.

Aggregating the smaller, FreeSurfer-defined regions into larger regions is another potential limitation to the study. The data for small regions were noisy and did not typically follow a sigmoidal trajectory. Perhaps in a larger or more cognitively diverse cohort, sigmoidal functions could be fit for smaller regions. Similarly, the ideal way to compare ε4 carriers and noncarriers would be to fit separate quadratics. The noncarriers in this sample, however, did not fit a quadratic probably because of lower levels of Aβ in the noncarriers in particular. In a larger sample, or one with impaired individuals, there may be enough noncarriers with high accumulation rates, which would allow for the fitting of 2 separate quadratics.

In the Aβ-tau analyses, we chose to use a liberal threshold of $p < 0.05$, not correcting for multiple comparisons, to visualize our results. This analysis was meant primarily to show the patterns of elevated tau regions in relation to regional accumulation of Aβ, rather than to directly compare the extent of tau deposition associated with accumulation of Aβ in each region. Because of this liberal threshold, we cannot claim from these analyses that accumulation of Aβ in one region leads to higher tau than any other region. In fact, though, the results again indicate to us greater regional similarities than differences in the relationships between where Aβ increases over time, and where tau deposits.

Finally, it is well known that Aβ-PET imaging is limited by the fact that it can only show us the location of Aβ plaques, which follow an earlier, oligomeric form of Aβ that is considered more toxic (Sakono and Zako, 2010; Salahuddin et al., 2016). It is possible that the reason for inconsistencies in “early regions” or findings such as those in the present study that amyloid appears to arise near-simultaneously in many brain regions, is due to

PETs inability to image the very early phases of Aβ accumulation. However, there is currently no method to image oligomeric Aβ.

5. Conclusions

This study indicates that Aβ accumulates nearly simultaneously throughout the brain in cognitively normal older adults. Global Aβ accumulation follows a sigmoidal trajectory over time, and the time of peak accumulation of Aβ of different brain regions can be placed on that trajectory within a 4-year span, peaking approximately 24–28 years after participants reach the mean baseline Aβ burden of cognitively normal, Aβ-negative older adults. Furthermore, faster rates of regional Aβ accumulation throughout the brain are associated with APOE ε4 allele carriage. Finally, faster accumulation of Aβ in nearly all regions was associated with elevated tau pathology, particularly in the temporal and parietal lobes, with little difference based on where Aβ accumulates. These results indicate that Aβ is unlikely to spread from one region to another, at least early in the disease process, but rather arises quickly across the brain perhaps based on shared molecular vulnerability. In addition, this study shows that those who have faster rates of Aβ accumulation not only have elevated genetic risk for sporadic, late-onset AD, but also exhibit elevated burden of a second hallmark of AD, tau pathology.

Acknowledgements

This work was supported by the National Institutes of Health (AG034570 and AG062542). Avid Radiopharmaceuticals enabled the use of the ^{18}F-Flortaucipir tracer but did not provide direct funding and were not involved in data analysis or interpretation.

Disclosure statement

Molly R. LaPoint – conceptualization, methodology, software, formal analysis, data curation, writing-original draft, visualization; Suzanne L. Baker – software, methodology, data curation, writingreview and editing; Susan M. Landau – methodology, data curation, writing-review and editing; Theresa M. Harrison – software, writing-review and editing; William J. Jagust – conceptualization, methodology, writing-review and editing, supervision, funding acquisition. Suzanne L. Baker has consulted for Genentech. Susan M. Landau has served on the advisory board for KeifeRx. William J. Jagust has consulted for Biogen, Bioclinica and CuraSen. Molly R. LaPoint and Theresa M. Harrison have nothing to declare.

- We verify that the present manuscript has not been previously published or submitted to any other journal.
- All authors have approved this manuscript and its submission to *Neurobiology of Aging*.

References

Adams JN, Maass A, Harrison TM, Baker SL, Jagust WJ, 2019. Cortical tau deposition follows patterns of entorhinal functional connectivity in aging. Elife 8, 1–22. doi: 10.7554/eLife.49132.

Baker SL, Lockhart SN, Price JC, He M, Huesman RH, Schonhaut D, Faria J, Rabinovici G, Jagust WJ, 2017a. Reference tissue-based kinetic evaluation of 18F-AV-1451 for tau imaging. J. Nucl. Med 58, 332–338. doi: 10.2967/jnumed.116.175273. [PubMed: 27587706]

Baker SL, Maass A, Jagust WJ, 2017b. Considerations and code for partial volume correcting [18F]-AV-1451 tau PET data. Data Br 15, 648–657. doi: 10.1016/j.dib.2017.10.024.

Blautzik J, Brendel M, Sauerbeck J, Kotz S, Scheiwein F, Bartenstein P, Seibyl J, Rominger A, 2017. Reference region selection and the association between the rate of amyloid accumulation over time and the baseline amyloid burden. Eur. J. Nucl. Med. Mol. Imaging 44, 1364–1374. doi: 10.1007/s00259-017-3666-8. [PubMed: 28326436]

Braak H, Braak E, 1991. Neuropathological stageing of Alzheimer-related changes. Acta Neuropathol 82, 239–259. doi: 10.1007/BF00308809. [PubMed: 1759558]

Burnham SC, Laws SM, Budgeon CA, Doré V, Porter T, Bourgeat P, Buckley RF, Murray K, Ellis KA, Turlach BA, Salvado O, Ames D, Martins RN, Rentz D, Masters CL, Rowe CC, Villemagne VL, 2020. Impact of APOE-ε4 carriage on the onset and rates of neocortical Aβ-amyloid deposition. Neurobiol. Aging 95, 46–55. doi: 10.1016/j.neurobiolaging.2020.06.001. [PubMed: 32750666]

Cho H, Choi JY, Hwang MS, Kim YJ, Lee HM, Lee HS, Lee JH, Ryu YH, Lee MS, Lyoo CH, 2016. In vivo cortical spreading pattern of tau and amyloid in the Alzheimer disease spectrum. Ann. Neurol 80, 247–258. doi: 10.1002/ana.24711. [PubMed: 27323247]

Elman JA, Oh H, Madison CM, Baker SL, Vogel JW, Marks SM, Crowley S, O'Neil JP, Jagust WJ, 2014. Neural compensation in older people with brain amyloid-β deposition. Nat. Neurosci 17, 1316–1318. doi: 10.1038/nn.3806. [PubMed: 25217827]

Fouquet M, Besson FL, Gonneaud J, La Joie R, Chételat G, 2014. Imaging brain effects of APOE4 in cognitively normal individuals across the lifespan. Neuropsychol. Rev 24, 290–299. doi: 10.1007/s11065-014-9263-8. [PubMed: 25146994]

Franzmeier N, Neitzel J, Rubinski A, Smith R, Strandberg O, Ossenkoppele R, Hansson O, Ewers M, Weiner Michael, Aisen P, Petersen R, Jack CR, Jagust W, Trojanowki JQ, Toga AW, Beckett L, Green RC, Saykin AJ, Morris J, Shaw LM, Liu E, Montine T, Thomas RG, Donohue M, Walter S, Gessert D, Sather T, Jiminez G, Harvey D, Donohue M, Bernstein M, Fox N, Thompson P, Schuff N, DeCArli C, Borowski B, Gunter J, Senjem M, Vemuri P, Jones D, Kantarci K, Ward C, Koeppe RA, Foster N, Reiman EM, Chen K, Mathis C, Landau S, Cairns NJ, Householder E, Reinwald LT, Lee V, Korecka M, Figurski M, Crawford K, Neu S, Foroud TM, Potkin S, Shen L, Kelley F, Kim S, Nho K, Kachaturian Z, Frank R, Snyder PJ, Molchan S, Kaye J, Quinn J, Lind B, Carter R, Dolen S, Schneider LS, Pawluczyk S, Beccera M, Teodoro L, Spann BM, Brewer J, Vanderswag H, Fleisher A, Heidebrink JL, Lord JL, Petersen R, Mason SS, Albers CS, Knopman D, Johnson Kris, Doody RS, Meyer JV, Chowdhury M, Rountree S, Dang M, Stern Y, Honig LS, Bell KL, Ances B, Morris JC, Carroll M, Leon S, Householder E, Mintun MA, Schneider S, OliverNG A, Griffith R, Clark D, Geldmacher D, Brockington J, Roberson E, Grossman H, Mitsis E, deToledo-Morrell L, Shah RC, Duara R, Varon D, Greig MT, Roberts P, Albert M, Onyike C, D'Agostino D, Kielb S, Galvin JE, Pogorelec DM, Cerbone B, Michel CA, Rusinek H, de Leon MJ, Glodzik L, De Santi S, Doraiswamy PM, Petrella JR, Wong TZ, Arnold SE, Karlawish JH, Wolk D, Smith CD, Jicha G, Hardy P, Sinha P, Oates E, Conrad G, Lopez OL, Oakley MA, Simpson DM, Porsteinsson AP, Goldstein BS, Martin K, Makino KM, Ismail MS, Brand C, Mulnard RA, Thai G, Ortiz CMA, Womack K, Mathews D, Quiceno M, Arrastia RD, King R, Weiner M, Cook KM, DeVous M, Levey AI, Lah JJ, Cellar JS, Burns JM, Anderson HS, Swerdlow RH, Apostolova L, Tingus K, Woo E, Silverman DHS, Lu PH, Bartzokis G, Radford NRG, ParfittH F, Kendall T, Johnson H, Farlow MR, Hake AM, Matthews BR, Herring S, Hunt C, van Dyck CH, Carson RE, MacAvoy MG, Chertkow H, Bergman H, Hosein C, Black S, Stefanovic B, Caldwell C, Hsiung GYR, Feldman H, Mudge B, Past MA, Kertesz A, Rogers J, Trost D, Bernick C, Munic D, Kerwin D, Mesulam MM, Lipowski K, Wu CK, Johnson N, Sadowsky C, Martinez W, Villena T, Turner RS, Johnson Kathleen, Reynolds B, Sperling RA, Johnson KA, Marshall G, Frey M, Yesavage J, Taylor JL, Lane B, Rosen A, Tinklenberg J, Sabbagh MN, Belden CM, Jacobson SA, Sirrel SA, Kowall N, Killiany R, Budson AE, Norbash A, Johnson PL, Obisesan TO, Wolday S, Allard J, Lerner A, Ogrocki P, Hudson L, Fletcher E, Carmichael O, Olichney J, DeCarli C, Kittur S, Borrie M, Lee TY, Bartha R, Johnson S, Asthana S, Carlsson CM, Potkin SG, Preda A, Nguyen D, Tariot P, Fleisher A, Reeder S, Bates V, Capote H, Rainka M, Scharre DW, Kataki M, Adeli A, Zimmerman EA, Celmins D, Brown AD, Pearlson GD, Blank K, Anderson K, Santulli RB, Kitzmiller TJ, Schwartz ES, SinkS KM, Williamson JD, Garg P, Watkins F, Ott BR, Querfurth H, Tremont G, Salloway S, Malloy P, Correia S, Rosen HJ, Miller BL, Mintzer J, Spicer K, Bachman D, Finger E, Pasternak S, Rachinsky I, Rogers J, Kertesz A, Drost D, Pomara N, Hernando R, Sarrael A, Schultz SK, Ponto LLB, Shim H, Smith KE, Relkin N, Chaing G, Raudin L, Smith A, Fargher K, Raj BA, 2020. Functional brain architecture is associated with the rate of tau accumulation in Alzheimer's disease. Nat. Commun 11, 1–17. doi: 10.1038/s41467-019-14159-1. [PubMed: 31911652]

Grothe MJ, Barthel H, Sepulcre J, Dyrba M, Sabri O, Teipel SJ, 2017. In vivo staging of regional amyloid deposition. Neurology 89, 2031–2038. doi: 10.1212/WNL.0000000000004643. [PubMed: 29046362]

Grothe MJ, Sepulcre J, Gonzalez-Escamilla G, Jelistratova I, Schöll M, Hansson O, Teipel SJ, 2018. Molecular properties underlying regional vulnerability to Alzheimer's disease pathology. Brain 141, 2755–2771. doi: 10.1093/brain/awy189. [PubMed: 30016411]

Guo T, Brendel M, Grimmer T, Rominger A, Yakushev I, 2017. Predicting regional pattern of longitudinal β-amyloid accumulation by baseline PET. J. Nucl. Med 58, 639–645. doi: 10.2967/jnumed.116.176115. [PubMed: 27754901]

Guo T, Dukart J, Brendel M, Rominger A, Grimmer T, Yakushev I, 2018. Rate of β-amyloid accumulation varies with baseline amyloid burden: Implications for anti-amyloid drug trials. Alzheimer's Dement 14, 1387–1396. doi: 10.1016/j.jalz.2018.05.013. [PubMed: 30420035]

He Z, Guo JL, McBride JD, Narasimhan S, Kim H, Changolkar L, Zhang B, Gathagan RJ, Yue C, Dengler C, Stieber A, Nitla M, Coulter DA, Abel T, Brunden KR, Trojanowski JQ, Lee VMY, 2018. Amyloid-β plaques enhance Alzheimer's brain tau-seeded pathologies by facilitating neuritic plaque tau aggregation. Nat. Med 24, 29–38. doi: 10.1038/nm.4443. [PubMed: 29200205]

Insel PS, Mormino EC, Aisen PS, Thompson WK, Donohue MC, 2020. Neuroanatomical spread of amyloid β and tau in Alzheimer's disease: implications for primary prevention. Brain Commun 2, 1–11. doi: 10.1093/braincomms/fcaa007.

Jack CR, Bennett DA, Blennow K, Carrillo MC, Dunn B, Haeberlein SB, Holtzman DM, Jagust W, Jessen F, Karlawish J, Liu E, Molinuevo JL, Montine T, Phelps C, Rankin KP, Rowe CC, Scheltens P, Siemers E, Snyder HM, Sperling R, Elliott C, Masliah E, Ryan L, 2018. NIA-AA research framework: toward a biological definition of alzheimer's disease. Alzheimer's dement. Silverberg, N, 14, 535–562. doi: 10.1016/j.jalz.2018.02.018.

Jack CR, Lowe VJ, Senjem ML, Weigand SD, Kemp BJ, Shiung MM, Knopman DS, Boeve BF, Klunk WE, Mathis CA, Petersen RC, 2008. 11C PiB and structural MRI provide complementary information in imaging of Alzheimer's disease and amnestic mild cognitive impairment. Brain 131, 665–680. doi: 10.1093/brain/awm336. [PubMed: 18263627]

Jack CR, Wiste HJ, Lesnick TG, Weigand SD, Knopman DS, Vemuri P, Pankratz VS, Senjem ML, Gunter JL, Mielke MM, Lowe VJ, Boeve BF, Petersen RC, 2013. Brain β-amyloid load approaches a plateau. Neurology 80, 890–896. doi: 10.1212/WNL.0b013e3182840bbe. [PubMed: 23446680]

Jagust WJ, Landau SM, 2021. Temporal dynamics of beta-amyloid accumulation in aging and Alzheimer's disease. Neurology doi:10.1212/WNL.0000000000011524

Jelistratova I, Teipel SJ, Grothe MJ, 2020. Longitudinal validity of PET-based staging of regional amyloid deposition. Hum. Brain Mapp 1–13. doi: 10.1002/hbm.25121.

Johnson KA, Schultz A, Betensky RA, Becker JA, Sepulcre J, Rentz D, Mormino E, Chhatwal J, Amariglio R, Papp K, Marshall G, Albers M, Mauro S, Pepin L, Alverio J, Judge K, Philiossaint M, Shoup T, Yokell D, Dickerson B, Gomez-Isla T, Hyman B, Vasdev N, Sperling R, 2016. Tau positron emission tomographic imaging in aging and early Alzheimer disease. Ann. Neurol 79, 110–119. doi: 10.1002/ana.24546. [PubMed: 26505746]

Klunk WE, Koeppe RA, Price JC, Benzinger TL, Devous MD, Jagust WJ, Johnson KA, Mathis CA, Minhas D, Pontecorvo MJ, Rowe CC, Skovronsky DM, Mintun MA, 2015. The centiloid project: standardizing quantitative amyloid plaque estimation by PET. Alzheimer's dement 11, 1–15.e4. doi:10.1016/j.jalz.2014.07.003 [PubMed: 25443857]

Leal SL, Lockhart SN, Maass A, Bell RK, Jagust WJ, 2018. Subthreshold amyloid predicts tau deposition in aging. J. Neurosci 38, 4 482–4 489. doi: 10.1523/JNEUROSCI.0485-18.2018.

Lim YY, Mormino EC, 2017. APOE genotype and early β-amyloid accumulation in older adults without dementia. Neurology 89, 1028–1034. doi: 10.1212/WNL.0000000000004336. [PubMed: 28794245]

Lockhart SN, Schöll M, Baker SL, Ayakta N, Swinnerton KN, Bell RK, Mellinger TJ, Shah VD, O'Neil JP, Janabi M, Jagust WJ, 2017. Amyloid and tau PET demonstrate region-specific associations in normal older people. Neuroimage 150, 191–199. doi: 10.1016/j.neuroimage.2017.02.051. [PubMed: 28232190]

Logan J, Fowler JS, Volkow ND, Wang G-J, Ding Y-S, Alexoff DL, 1996. Distribution volume ratios without blood sampling from graphical analysis of PET data. J. Cereb. Blood Flow Metab 16, 834–840. [PubMed: 8784228]

Lopresti BJ, Campbell EM, Yu Z, Anderson SJ, Cohen AD, Minhas DS, Snitz BE, Royse SK, Becker CR, Aizenstein HJ, Mathis CA, Lopez OL, Klunk WE, Tudorascu DL, 2020. Influence of apolipoprotein-E genotype on brain amyloid load and longitudinal trajectories. Neurobiol. Aging 94, 111–120. doi: 10.1016/j.neurobiolaging.2020.05.012. [PubMed: 32603776]

Mathis CA, Wang Y, Holt DP, Huang GF, Debnath ML, Klunk WE, 2003. Synthesis and evaluation of 11C-labeled 6-substituted 2-arylbenzothiazoles as amyloid imaging agents. J. Med. Chem 46, 2740–2754. doi: 10.1021/jm030026b. [PubMed: 12801237]

Mattsson N, Palmqvist S, Stomrud E, Vogel J, Hansson O, 2019. Staging β - amyloid pathology with amyloid positron emission tomography. JAMA Neurol 76, 1319–1329. doi: 10.1001/jamaneurol.2019.2214. [PubMed: 31314895]

Mishra S, Blazey TM, Holtzman DM, Cruchaga C, Su Y, Morris JC, Benzinger TLS, Gordon BA, 2018. Longitudinal brain imaging in preclinical Alzheimer disease: impact of APOE 4 genotype. Brain 141, 1828–1839. doi: 10.1093/brain/awy103. [PubMed: 29672664]

Mormino EC, Kluth JT, Madison CM, Rabinovici GD, Baker SL, Miller BL, Koeppe RA, Mathis CA, Weiner MW, Jagust WJ, 2009. Episodic memory loss is related to hippocampal-mediated β-amyloid deposition in elderly subjects. Brain 132, 1310–1323. doi: 10.1093/brain/awn320. [PubMed: 19042931]

Mormino EC, Smiljic A, Hayenga AOH, Onami S, Greicius MD, Rabinovici GD, Janabi M, Baker SLV, Yen I, Madison CM, Miller BL, Jagust WJ, 2011. Relationships between beta-amyloid and functional connectivity in different components of the default mode network in aging. Cereb. Cortex 21, 2399–2407. doi: 10.1093/cercor/bhr025. [PubMed: 21383234]

Oh H, Madison C, Baker S, Rabinovici G, Jagust W, 2016. Dynamic relationships between age, amyloid-β deposition, and glucose metabolism link to the regional vulnerability to Alzheimer's disease. Brain 139, 2275–2289. doi: 10.1093/brain/aww108. [PubMed: 27190008]

Palmqvist S, Schöll M, Strandberg O, Mattsson N, Stomrud E, Zetterberg H, Blennow K, Landau S, Jagust W, Hansson O, 2017. Earliest accumulation of β-amyloid occurs within the default-mode network and concurrently affects brain connectivity. Nat. Commun 8. doi: 10.1038/s41467-017-01150-x.

Pascoal TA, Mathotaarachchi S, Shin M, Benedet AL, Mohades S, Wang S, Beaudry T, Kang MS, Rosa-Neto P, Benedet AL, Soucy JP, Labbe A, Labbe A, Gauthier S, 2017. Synergistic interaction between amyloid and tau predicts the progression to dementia. Alzheimer's Dement 13, 644–653. doi: 10.1016/j.jalz.2016.11.005. [PubMed: 28024995]

Price JC, Klunk WE, Lopresti BJ, Lu X, Hoge JA, Ziolko SK, Holt DP, Meltzer CC, DeKosky ST, Mathis CA, 2005. Kinetic modeling of amyloid binding in humans using PET imaging and Pittsburgh compound-B. J. Cereb. Blood Flow Metab 25, 1528–1547. doi: 10.1038/sj.jcbfm.9600146. [PubMed: 15944649]

Resnick SM, Bilgel M, Moghekar A, An Y, Cai Q, Wang MC, Thambisetty M, Prince JL, Zhou Y, Soldan A, Wong DF, O'Brien RJ, Ferrucci L, Albert MS, 2015. Changes in Aβ biomarkers and associations with APOE genotype in 2 longitudinal cohorts. Neurobiol. Aging 36, 2333–2339. doi: 10.1016/j.neurobiolaging.2015.04.001. [PubMed: 26004017]

Rousset OG, Ma Y, Evans AC, 1998. Correction for partial volume effects in PET: principle and validation. J correction for partial volume effects in PET: principle and validation. J. Nucl. Med 39, 904–911. [PubMed: 9591599]

Sakono M, Zako T, 2010. Amyloid oligomers: formation and toxicity of Aβ oligomers. FEBS J 277, 1348–1358. doi: 10.1111/j.1742-4658.2010.07568.x. [PubMed: 20148964]

Sakr FA, Grothe MJ, Cavedo E, Jelistratova I, Habert MO, Dyrba M, Gonzalez-Escamilla G, Bertin H, Locatelli M, Lehericy S, Teipel S, Dubois B, Hampel H, 2019. Applicability of in vivo staging of regional amyloid burden in a cognitively normal cohort with subjective memory complaints: The INSIGHT-preAD study. Alzheimer's Res. Ther 11, 1–11. doi: 10.1186/s13195-019-0466-3. [PubMed: 30611304]

Salahuddin P, Fatima MT, Abdelhameed AS, Nusrat S, Khan RH, 2016. Structure of amyloid oligomers and their mechanisms of toxicities: targeting amyloid oligomers using novel therapeutic

approaches. Eur. J. Med. Chem 114, 41–58. doi: 10.1016/j.ejmech.2016.02.065. [PubMed: 26974374]

Schöll M, Lockhart SN, Schonhaut DR, O'Neil JP, Janabi M, Ossenkoppele R, Baker SL, Vogel JW, Faria J, Schwimmer HD, Rabinovici GD, Jagust WJ, 2016. PET imaging of tau deposition in the aging human brain. Neuron 89, 971–982. doi: 10.1016/j.neuron.2016.01.028. [PubMed: 26938442]

Sperling RA, Aisen PS, Beckett LA, Bennett DA, Craft S, Fagan AM, Iwatsubo T, Jack CR, Kaye J, Montine TJ, Park DC, Reiman EM, Rowe CC, Siemers E, Stern Y, Yaffe K, Carrillo MC, Thies B, Morrison-bogorad M, Wagster MV, Phelps CH, 2011. Toward defining the preclinical stages of Alzheimer's disease: recommendations from the national institute on aging-Alzheimer's association workgroups on diagnostic guidelines for Alzheimer's disease. Alzheimer's Dement 7, 280–292. doi: 10.1016/j.jalz.2011.03.003. [PubMed: 21514248]

Teipel SJ, Dyrba M, Chiesa PA, Sakr F, Jelistratova I, Lista S, Vergallo A, Lemercier P, Cavedo E, Habert MO, Dubois B, Hampel H, Grothe MJ, 2020. In vivo staging of regional amyloid deposition predicts functional conversion in the preclinical and prodromal phases of Alzheimer's disease. Neurobiol. Aging 93, 98–108. doi: 10.1016/j.neurobiolaging.2020.03.011. [PubMed: 32291113]

Thal DR, Rüb U, Orantes M, Braak H, 2002. Phases of Aβ-deposition in the human brain and its relevance for the development of AD. Neurology 58, 1791–1800. [PubMed: 12084879]

Tosun D, Landau S, Aisen PS, Petersen RC, Mintun M, Jagust W, Weiner MW, 2017. Association between tau deposition and antecedent amyloid-β accumulation rates in normal and early symptomatic individuals. Brain 140, 1499–1512. doi: 10.1093/brain/awx046. [PubMed: 28334939]

Vemuri P, Lowe VJ, Knopman DS, Senjem ML, Kemp BJ, Schwarz CG, Przybelski SA, Machulda MM, Petersen RC, Jack CR, 2017. Tau-PET uptake: Regional variation in average SUVR and impact of amyloid deposition. Alzheimer's Dement. Diagnosis, Assess. Dis. Monit 6, 21–30. doi: 10.1016/j.dadm.2016.12.010.

Villemagne VL, Burnham S, Bourgeat P, Brown B, Ellis KA, Salvado O, Szoeke C, Macaulay SL, Martins R, Maruff P, Ames D, Rowe CC, Masters CL, 2013. Amyloid β deposition, neurodegeneration, and cognitive decline in sporadic Alzheimer's disease: a prospective cohort study. Lancet Neurol 12, 357–367. doi: 10.1016/S1474-4422(13)70044-9. [PubMed: 23477989]

Villeneuve S, Rabinovici GD, Cohn-Sheehy BI, Madison C, Ayakta N, Ghosh PM, Joie R. La, Arthur-bentil SK, Vogel JW, Marks SM, Lehmann M, Rosen HJ, Reed B, Olichney J, Boxer AL, Miller BL, Borys E, Jin L, Huang EJ, Grinberg LT, Decarli C, Seeley WW, Jagust W, 2015. Existing Pittsburgh compound-B positron emission tomography thresholds are too high: statistical and pathological evaluation. Brain 138, 2020–2033. doi: 10.1093/brain/awv112. [PubMed: 25953778]

Vlassenko AG, Vaishnavi SN, Couture L, Sacco D, Shannon BJ, Mach RH, Morris JC, Raichle ME, Mintun MA, 2010. Spatial correlation between brain aerobic glycolysis and amyloid-β (Aβ) deposition. Proc. Natl. Acad. Sci. U. S. A 107, 17763–17767. doi: 10.1073/pnas.1010461107. [PubMed: 20837517]

Vogel JW, Iturria-Medina Y, Strandberg OT, Smith R, Levitis E, Evans AC, Hansson O, 2020. Spread of pathological tau proteins through communicating neurons in human Alzheimer's disease. Nat. Commun 11, 2612. doi: 10.1038/s41467-020-15701-2. [PubMed: 32457389]

Whittington A, Sharp DJ, Gunn RN, 2018. Spatiotemporal distribution of B-Amyloid in Alzheimer disease is the result of heterogeneous regional carrying capacities. J. Nucl. Med 59, 822–827. doi: 10.2967/jnumed.117.194720. [PubMed: 29146694]

Yotter RA, Doshi J, Clark V, Sojkova J, Zhou Y, Wong DF, Ferrucci L, Resnick SM, Davatzikos C, 2013. Memory decline shows stronger associations with estimated spatial patterns of amyloid deposition progression than total amyloid burden. Neurobiol. Aging 34, 2835–2842. doi: 10.1016/j.neurobiolaging.2013.05.030.Memory. [PubMed: 23859610]

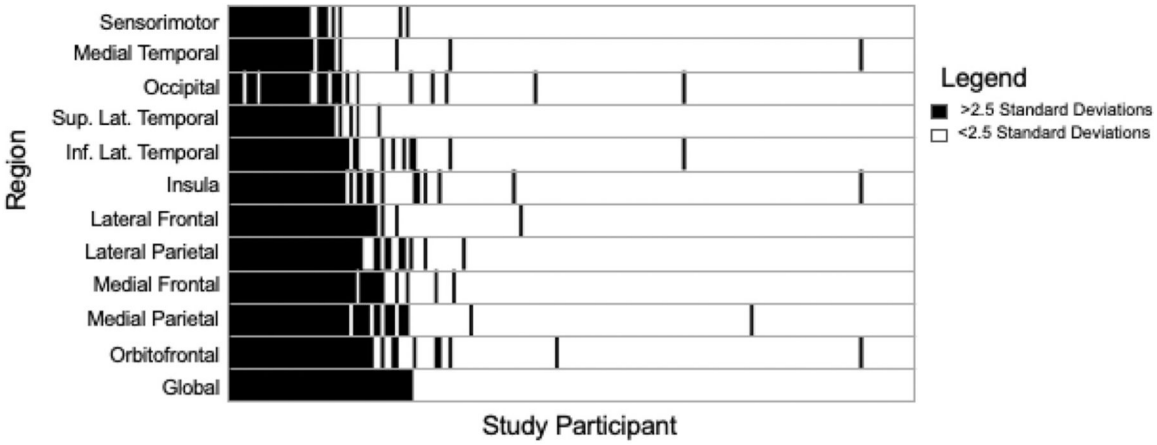

Fig. 1.

Regional PIB by subject using cross-sectional Z-score method. In this figure, each participant is represented on the x-axis, in descending order by their global PIB DVR, and the regions are listed with on the y-axis. For each participant, the regions with a Z-score above 2.5 standard deviations are filled in black. Most participants who have elevated PIB-PET in one region have it in most or all other regions.

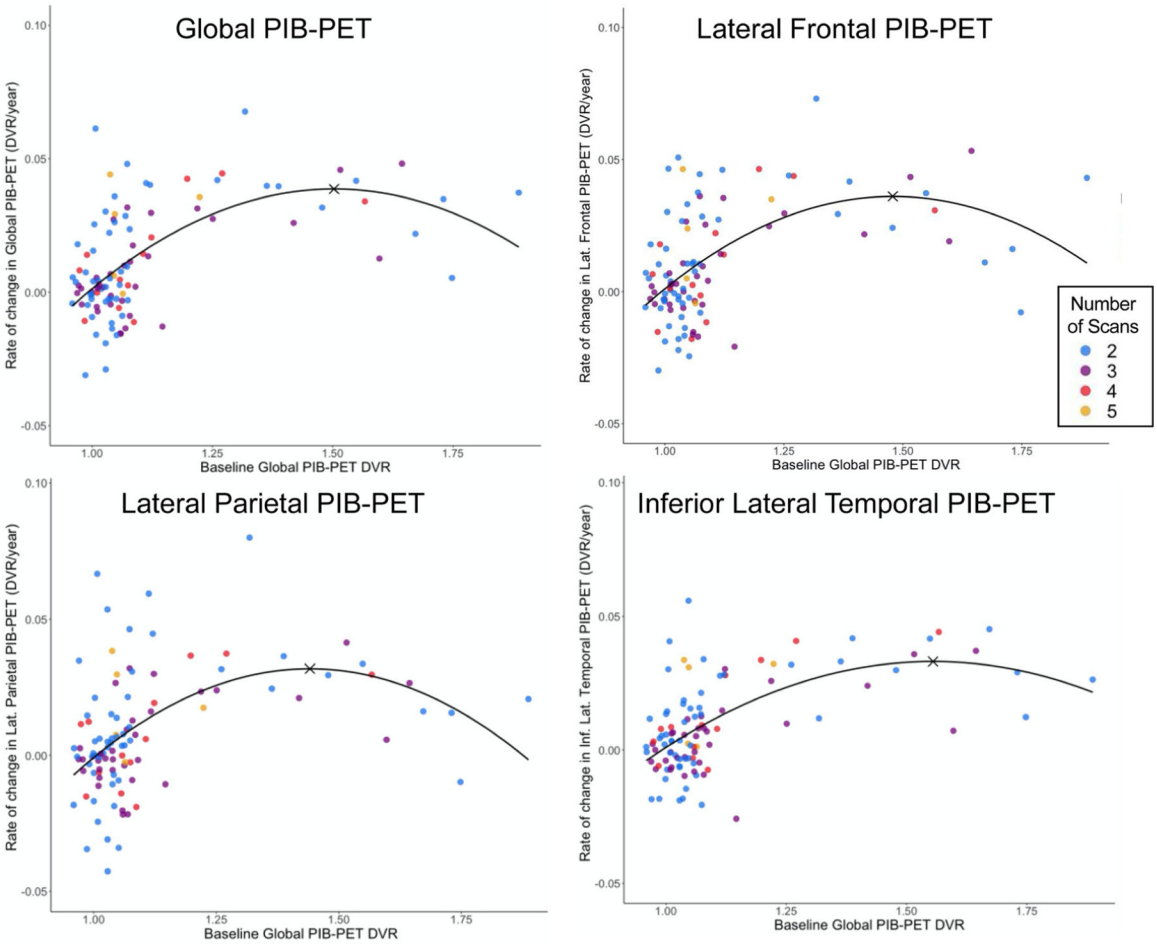

Fig. 2.

Quadratic Fit for a subset of regions. These figures show the relationships between global PIB at baseline and regional accumulation of amyloid for a subset of the analyzed regions. Global PIB is on the x-axis and regional change (DVR/year) is on the y-axis. Study participants are color coded according to how many PIB scans they have received. The black “X” on each graph is the point at which the regional slope is at its maximum. After this time point, regional PIB begins to decelerate.

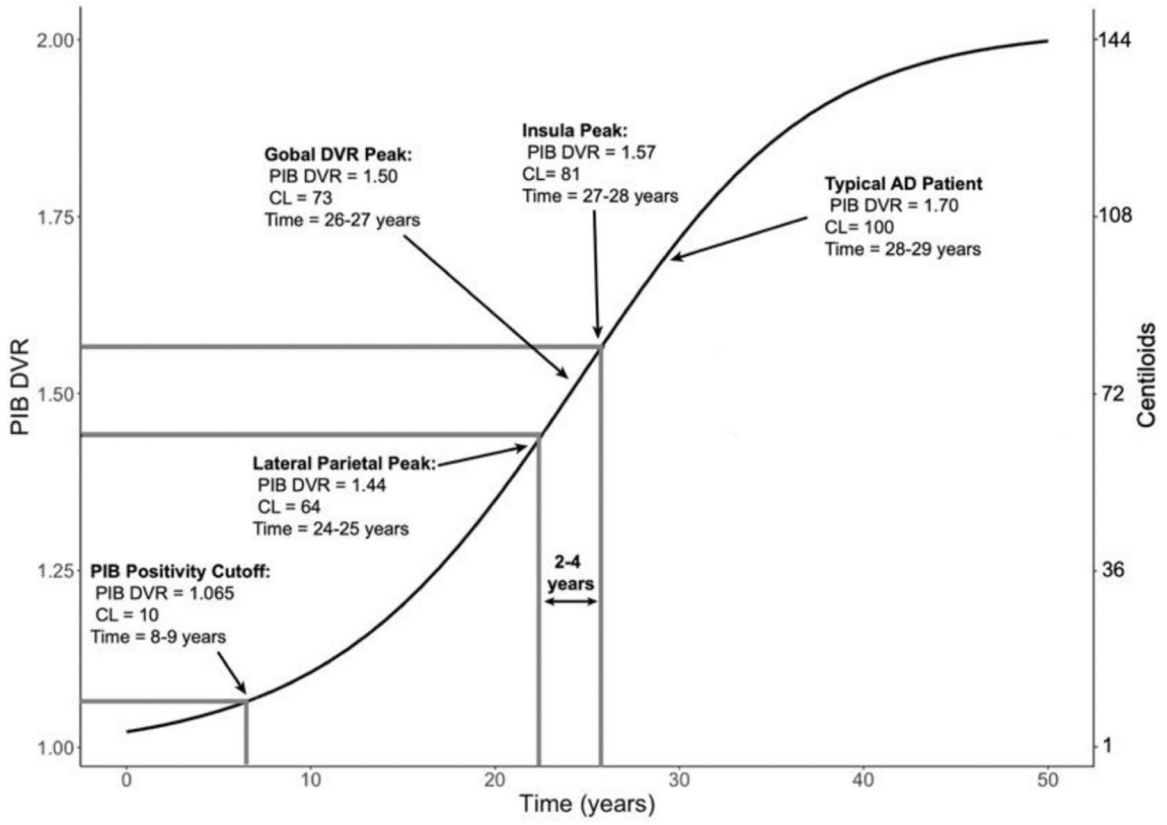

Fig. 3.

Sigmoidal time-global PIB relationship, showing different points of interest. This figure shows how global PIB DVR changes (y-axis) over 50 years, starting with the mean PIB DVR of amyloid-negative participants in the current study (DVR = 1.02). It takes 8–9 years to reach a DVR of 1.065, the cutoff for PIB positivity in this sample, and the 8 different regions reach their peak accumulation rates between 24 and 28 years from the mean baseline.

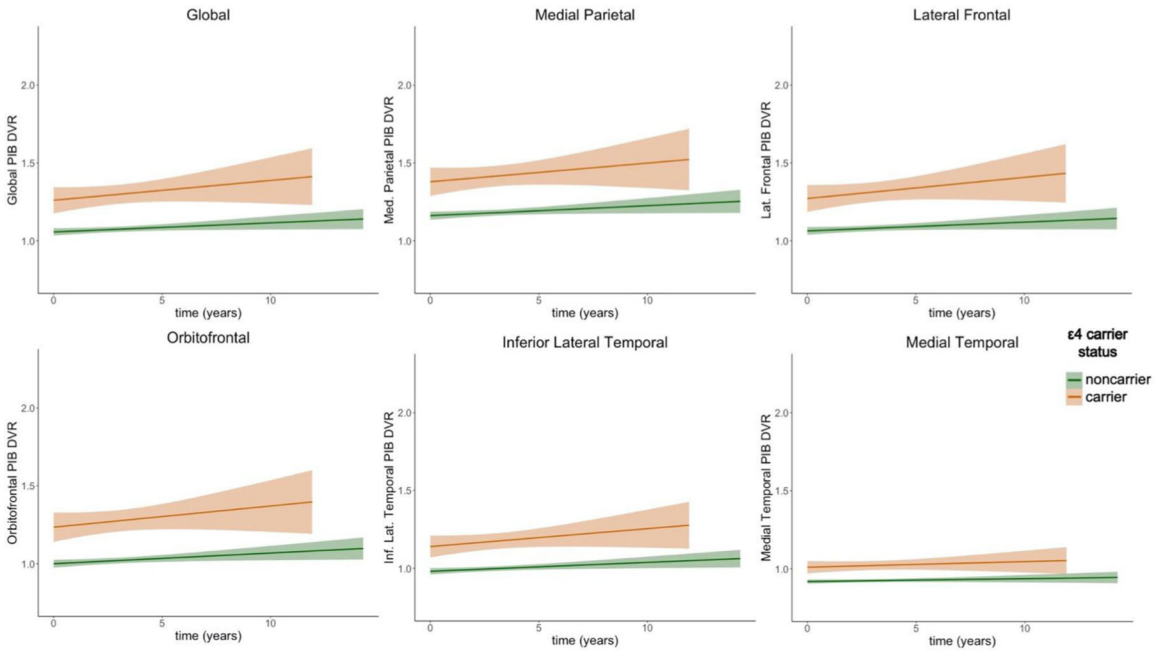

Fig. 4.

PIB accumulation rates in ε4 carriers versus noncarriers. These plots show the accumulation over time in ε4 carriers versus noncarriers. ε4 carriers have significantly faster accumulation in all regions (see Table 4), controlling for baseline age and sex, and both terms interacting with time, in the linear mixed effects models. These figures are showing linear model fits in each group, not including any covariates.

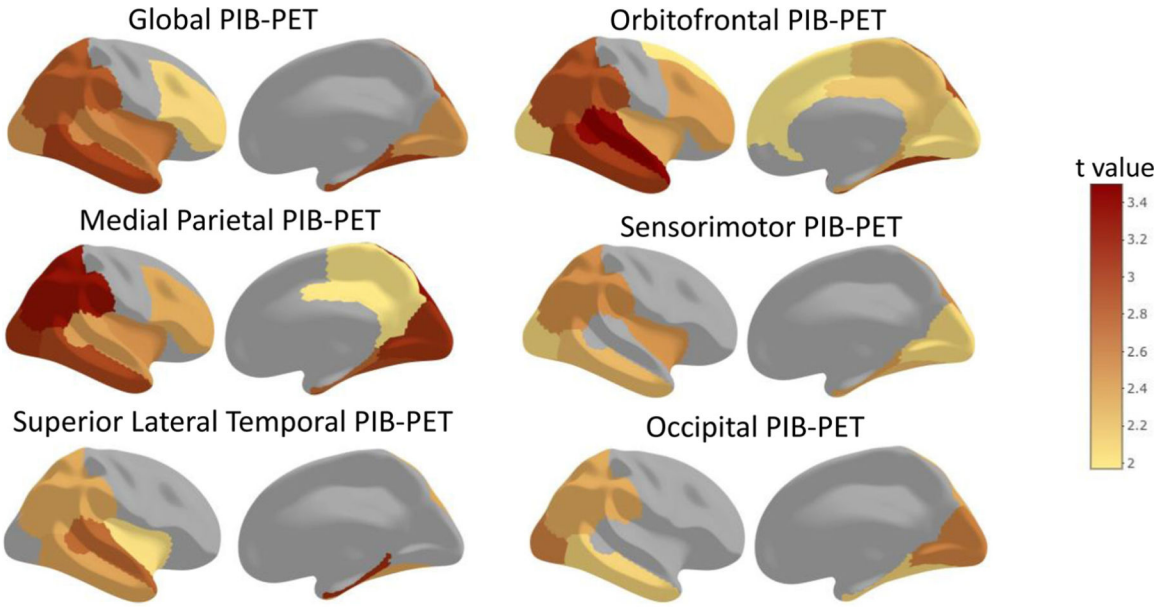

Fig. 5.

PIB-Tau relationships. Colors reflect the association between regional Aβ accumulation rates in the indicated brain region and regional FTP-PET at a liberal threshold of $p <$ 0.05, without correction for multiple comparisons. The pattern of associations between Aβ accumulation rates and tau deposition is similar across regions, with the strongest PIB-FTP relationships in temporal and lateral parietal regions and more moderate associations in global, OFC, and medial parietal PIB regions.

Table 1

Subject demographics and descriptive statistics. A summary of all study participants. Participants in the longitudinal sample are a subset of the cross-sectional sample, and the FTP-PET sample is a further subset of the longitudinal sample

Sample	Cross-sectional	Longitudinal	FTP-PET
N	195	106	88
Female/Male	112/83	66/40	54/34
Age (y)	75.5 ± 5.97	75.0 ± 5.13	74.6 ± 4.93
Y of Education	16.9 ± 2.33	16.8 ± 1.86	17.0 ±2.54
Follow-up Time (y)	-	4.71 ± 3.07	4.91 ± 3.24
Number PIB scans (2,3,4,5)	-	52, 35, 13, 5	38, 32, 13, 5
PIB+/−	73/122	41/65	35/53
E4 carriers/noncarriers	45/134 (16 missing)	31/74 (1 missing)	25/62 (1 missing)

Table 2

Z-score method results. Cross-sectional analyses ranked regions based on the number of participants with elevated Aβ in each region. Elevated Aβ was defined as having a Z-score value above 2.5 standard deviations, based on the Aβ-negative participants.

Region	Percent Involvement	Z-score mean
Global PIB	26.7%	2.87
OFC	25.6%	2.16
Medial Parietal	25.1%	2.12
Medial Frontal	24.1%	2.16
Lateral Parietal	23.1%	1.85
Lateral Frontal	23.1%	2.43
Insula	23.1%	1.60
Inferior Lateral Temporal	22.1%	2.21
Superior Lateral Temporal	17.4%	1.59
Occipital	17.4%	1.01
MTL	16.9%	0.98
Sensorimotor	15.4%	1.08

Table 3

Global PIB value at which each region reaches its peak accumulation rate. This table shows the global PIB DVR, Mean regional slope calculated with linear regression, Global PIB Centiloid value at peak, and number of years it takes for each region to reach its peak rate of accumulation using the quadratic fit. Parietal and frontal regions precede lateral temporal regions as well as the insula

Region	Global PIB DVR at peak regional slope	Mean slope (DVR/y)	Centiloid value at peak regional slope	Y to Peak Accumulation Rate
Lateral Parietal	1.44	0.008	64	24–25
Sensorimotor	1.46	0.007	67	25–26
Medial Parietal	1.47	0.011	68	25–26
Medial Frontal	1.48	0.013	69	25–26
Lateral Frontal	1.48	0.010	69	25–26
Global PIB	1.50	0.011	73	26–27
Inferior Lateral Temporal	1.56	0.009	80	27–28
Superior Lateral Temporal	1.56	0.007	80	27–28
Insula	1.57	0.006	81	27–28

Table 4

Results from ε4 LME analyses. T and *p* values from the linear mixed effects models run comparing amyloid accumulation in ε4 carriers versus noncarriers. Included in the model were age and baseline time, both interacting with time, as covariates (not shown above). The ε4 × time term represents the difference over time in the trajectories of the 2 groups, and the ε4 term is the overall difference between ε4 carriers and noncarriers. The analyses were coded such that the direction of the results indicates that ε4 carriers had higher values and faster accumulation than the noncarriers

Region	ε4 × time termt value	ε4 × time term *p* value	ε4 termt value	ε4 term *p* value
Global PIB	4.86	$p < 0.0001$	5.41	$p < 0.0001$
OFC	4.16	$p < 0.0001$	5.79	$p < 0.0001$
Medial Parietal	3.97	$p = 0.0001$	5.06	$p < 0.0001$
Medial Frontal	4.10	$p = 0.0001$	5.10	$p < 0.0001$
Lateral Parietal	4.18	$p < 0.0001$	5.31	$p < 0.0001$
Lateral Frontal	5.10	$p < 0.0001$	5.43	$p < 0.0001$
Insula	4.52	$p < 0.0001$	4.80	$p < 0.0001$
Inferior Lateral Temporal	4.76	$p < 0.0001$	4.81	$p < 0.0001$
Superior Lateral Temporal	4.19	$p < 0.0001$	4.47	$p < 0.0001$
Occipital	3.93	$p = 0.0007$	3.93	$p = 0.002$
MTL	3.90	$p = 0.0001$	4.21	$p = 0.0001$
Sensorimotor	3.17	$p = 0.002$	3.93	$p = 0.0002$

Table 5

Comparison of papers modeling the time course of amyloid accumulation. A comparison of 4 papers (the present study and 3 others) that have modeled the time course of amyloid accumulation in the ADNI, Alzheimer's disease neuroimaging initiative; MCSA, the mayo clinic study of aging; and the AIBL, Australian imaging biomarkers, and lifestyle study.

Study	This paper	ADNI (Jagust & Landau 2021)	MCSA (Jack et al. 2013)	AIBL (Villemagne et al. 2013)
Sigmoid starting value	4 CL (AB- average)	4 CL (AB- average)	1.3 PIB SUVR	1.17 PIB SUVR (AB- average for accumulators)
Time from baseline to AB+ threshold	8–9 y25 CL	7 y25.3 CL	6.63 y (SUVR 1.5 to peak)	12 y
Time from AB+ threshold to peak	17–18 y	3 y	-	~17 y[a]
Time from peak to typical AD patient	3–4 y(94 CL)	18 y(100 CL)	7.66 y (peak to SUVR 2.5)	~2 y[a]

[a]Estimated from the papers' figures